A Model of Immediate Implant Placement to Evaluate Early Osseointegration in 129/Sv Diabetic Mice

Claudia Cristina Biguetti, DDS, MSc, PhD[1]/Alexandra Arteaga, BS, MS[2]/
Bhuvana Lakkasetter Chandrashekar, BS, MS[2]/Evelin Rios[2]/Ryan Margolis, BS, MS[2]/Danieli C. Rodrigues, BS, MS, PhD[2]

Purpose: To analyze the process of early oral osseointegration of titanium (Ti) implants in diabetic 129/Sv mice through microCT and histologic and immunohistochemical analysis. ***Materials and Methods:*** A group of 30 male 129/Sv mice was equally subdivided into two groups: *(1)* nondiabetic (ND), in which mice did not undergo systemic alterations and received a standard diet, and *(2)* diabetic (D), in which mice were provided a high-fat diet from the age of 6 weeks until the conclusion of the study and received two intraperitoneal (IP) injections of streptozotocin (STZ) at a concentration of 100 mg/Kg each. Each mouse underwent extraction of a maxillary first molar, and customized Ti screws (0.50 mm diameter, 1.5 mm length) were placed in the residual alveolar sockets of the palatal roots. At 7 and 21 days after implant placement, the animals were euthanized for maxilla and pancreas collection. Maxillae containing Ti implants were analyzed with microCT, histology, and immunohistochemistry for cells that were positive for F4/80, CD146, runt-related transcription factor 2 (Runx2), and proliferating cell nuclear antigen (PCNA). Pancreata were histologically analyzed. Quantitative data were statistically analyzed with a significance level at 5% ($P < .05$). ***Results:*** ND mice presented successful healing and osseointegration, with a significantly higher fraction of bone volume compared to D mice, both at the alveolar sockets (53.39 ± 5.93 and 46.08 ± 3.18, respectively) and at the implant sites (68.88 ± 7.07 and 44.40 ± 6.98, respectively) 21 days after implant placement. Histologic evaluation revealed that the ND mice showed a significant decrease in inflammatory infiltrate and a significant increase in newly formed bone matrix at 21 days, whereas peri-implant sites in the D mice were predominantly encapsulated by fibrous tissue and chronic inflammatory infiltrate. Immunohistochemical characterization revealed higher Runx2 osteoblast differentiation and higher cell proliferation activity in the ND mice at 7 days, while higher amounts of macrophages were present in D mice at 7 and 21 days. Interestingly, no differences were found in CD146-positive cells when comparing ND and D mice. ***Conclusions:*** This study evaluated the effects of immediate dental implant placement in 129/Sv diabetic mice by using specific healing markers to identify changes in cellular events involved in early oral osseointegration. This approach may serve as tool to evaluate new materials and surface coatings to improve osseointegration in diabetic patients. *Int J Oral Maxillofac Implants 2023;38:1200–1210. doi: 10.11607/jomi.10335*

Keywords: hyperglycemia, mouse, osseointegration, inflammation, bone

Diabetes mellitus (DM) is a prevalent metabolic disorder involving chronic hyperglycemia.[1] This disease affects about 34.2 million American adults (10.5% of the population) and 451 million adults worldwide. The worldwide population of adults with DM is expected to reach 693 million by 2045.[1] Both type 1 and type 2 DM negatively impact the immunologic[2] and skeletal systems,[3] leading to increased susceptibility to oral health deterioration, including an increased risk of periodontal disease, tooth loss, and implant failure.[4,5] Indeed, poorly controlled glycemia in diabetic persons is recognized as a potential risk factor for delayed osseointegration, increased peri-implant inflammation, and a poor prognosis for implant survival.[6] Diabetic individuals present higher implant failure rates (10%–20%) compared to nondiabetic patients (1%–3%).[7–9] Implant failure generates morbidity and loss of productivity, worsening health, and increasing financial burdens. High blood glucose levels and delayed osseointegration also elevate the risk for peri-implantitis.[10] Therefore, understanding the initial events involving the detrimental effects of hyperglycemia on early osseointegration could translate to the use of new targets to increase dental implant predictability in diabetic patients.

Clinical and preclinical studies have confirmed that the effects of both type 1 and type 2 DM on the

[1]Laboratory of Regenerative Medicine, Department of Biomechanics and Surgery, School of Podiatric Medicine, The University of Texas Rio Grande Valley, Harlingen, Texas, USA.
[2]Department of Bioengineering, The University of Texas at Dallas, Richardson, Texas, USA.

Correspondence to: Claudia Cristina Biguetti, DDS, MSc, PhD, School of Podiatric Medicine, The University of Texas Rio Grande Valley, 2102 Treasure Hills Blvd, Harlingen, TX 78550.
Email: claudia.biguetti@utrgv.edu

Submitted November 1, 2022; accepted January 16, 2023.

skeleton[11–13] diminish tissue healing/recovery capacity.[2,14,15] Mechanisms that lead to poor bone quality and healing are complex and involve a range of different factors, such as a defective immune response and poor inflammation resolution in injured sites.[2] A recent experimental study in diabetic mice demonstrated that stem cells within the periosteum have reduced proliferation capacity, which negatively affects the migration/proliferation of bone cell progenitors (ie, mesenchymal stem cells [MSCs]) into sites of healing, as a result of DM.[16] Although these studies were not performed in the presence of titanium (Ti) implants, it is reasonable to infer that these factors may also negatively affect the integration and stability of bone-implantable devices.

While incremental studies are useful to validate the consequences of DM in bone, there is still a need to identify specific markers of poor inflammation resolution and poor bone formation in peri-implant tissue. The specific use of mouse models offers the advantage of allowing proper dissection of the biologic mechanisms underlying inflammation and healing, thanks to the vast availability of efficient genetic, molecular, and pharmacologic tools.[17,18] In this respect, the cellular and molecular mechanisms underlying early Ti osseointegration have been comprehensively described in oral osseointegration models in mice and rats.[18] In general, the process of osseointegration in healthy implant hosts starts with a protein layer formation adhered to the Ti surface[19] and continues with a coordinated inflammatory response at the host/biomaterial interface.[18] The regulation of this initial inflammatory response toward resolution within 7 days of implant placement seems to be the determinant factor for successful bone differentiation in Ti thread spaces.[18,20] These initial steps are characterized by a higher expression of MSCs, regenerative macrophage markers, and osteoblast differentiation.[18] On the other hand, previous studies point to clues that impaired immunomodulation and a lack of signals for bone differentiation may also play a crucial role in poor Ti implant osseointegration outcomes and lack of implant stability, facilitating peri-implant disease development[21] or leading to impaired osseointegration in diabetic conditions.[22] Given the advantages of using mouse models in translational research applied to implant dentistry, it may be a valuable tool to investigate the pathophysiologic response underlying diabetes-induced impaired osseointegration.

The aim of this study was to develop and characterize a model of diabetic 129/Sv mice to investigate the cellular events underlying diabetes-induced impaired osseointegration. The molecular/microscopic evaluation of how this metabolic disease influences the immune response and the quality of osseointegration is essential for developing new therapeutic tools to prevent early implant failure in the diabetic population.

MATERIALS AND METHODS

Animals

All experimental procedures (diabetes induction and validation, implant placement surgeries, pre- and postoperative care, and euthanasia) were carried out with supervision and approval from the Institutional Animal Care and Use Committee (IACUC no. 21-08). A total of 30 6-week-old male wild-type 129/Sv mice was purchased from Charles River Laboratories (Wilmington, MA), and the mice were maintained in specific pathogen-free conditions in the vivarium at the University of Texas at Dallas (Richardson, TX). Following a minimum of 72 hours for acclimation and quarantine in the vivarium, the animals were equally distributed into two experimental groups: the nondiabetic (ND) control group and the diabetic (D) group. Sterile water and dry food pellets (Rodent Chow, Purina) were available to animals ad libitum, except for 72 hours following Ti implant surgery, during which the diet was crumbled and mixed with water. Following surgery, ND and D mice were distributed into two groups for euthanasia and sample collections at 7 and 21 days after surgery.

Experimental Protocol for DM Induction

This study employed a diabetic model using the 129/Sv mouse strain, which has been optimized for diabetes development.[23] A total of 15 mice from D group were randomly allocated to 5 cages with 3 animals per cage. The DM induction was performed using a combination of a high-fat diet (HFD) and two spaced intraperitoneal (IP) injections of streptozotocin (STZ, S-0130, Sigma-Aldrich). This protocol resulted in less distress in the animals (only two injections) and decreased complications compared to several alternatives in the literature.[23,24] In brief, an HFD (Purina Lab Diet 5008) was introduced from 6 weeks of age until the conclusion of the study. STZ (100 mg/kg) was injected when the mice reached 10 weeks of age and weighed > 24 g. Mice were fasted for 4 hours prior to STZ injection (8AM to 12PM) and were fed with softened food during the first 7 days after the STZ injections to decrease acute complications related to weight loss.[24] Animals were weighed, and STZ doses were subsequently calculated based on individual weights. Immediately prior to injection, STZ was reconstituted in cold 1X phosphate-buffered saline (PBS), and mice received IP STZ 100 mg/kg in volumes ranging from 220 to 228 µL, according to weight. Mice received two STZ injections of 100 mg/kg within a 72-hour interval.[23,24] As a control, three ND mice were fasted and treated with 220 to 228 µL of cold 1X PBS within a 72-hour interval. Fasting plasma glucose levels (FPGL, mg/dL) and surgeries occurred 7 days after the final STZ injection.

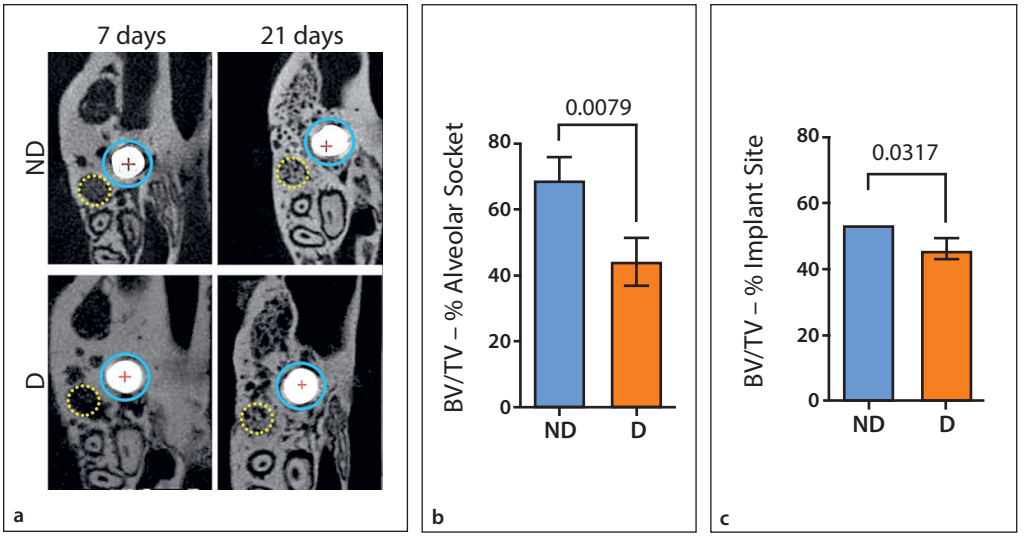

Fig 1 MicroCT analysis of alveolar sockets and implantation sites in 129/Sv ND and D mice. *(a)* Coronal section of the right hemimaxilla showing the implant location *(blue circle)* in the palatine root socket and the vestibular distal root *(dashed yellow line)* at 7 and 21 days. The BV/TV fraction was calculated with data at 21 days. Results are presented as mean ± SD for BV/TV (%) of newly formed bone at *(b)* the vestibular distal socket and *(c)* the peri-implant sites.

Validation of DM Protocol in 129/Sv Mice

All ND and D mice were weighed both upon arrival at the vivarium and before all experimental procedures. For FPGL measurements, ND and D animals were fasted for 4 hours prior to the procedure. Each procedure involving injection or vein puncture (ie, the STZ injection or puncture for blood glucose measurement) was performed with the animal pre-anesthetized by inhalation of 4% isoflurane to avoid increased animal distress and variations in glucose levels. Blood was collected from the tail vein in a glucose strip and FPGL (mg/dL) was measured with a glucometer (AlphaTRAK 2 Blood Glucose Monitoring System Kit, Zoetis Petcare). FPGL was measured in ND and D mice groups before major experimental procedures at the first STZ injection (ND mice were evaluated as controls), after 7 days of both doses of STZ, prior to implant placement, and prior to euthanasia. According to the literature, mice presenting with FPGL > 250 mg/dL at day 7 after the last STZ dose were considered diabetic, whereas normal FPGL and prediabetes were defined as < 200 mg/dL and between 200 and 250 mg/dL, respectively.[25] After euthanasia, pancreas samples from ND and D mice were collected to be evaluated via histopathologic analysis.

Implants

Commercially pure Ti, machined surface threaded dentin screws (ø 0.50 mm × 2 mm, Fairfax Dental), were customized to be used as dental implants in this study. Orthodontic pliers were used to cut all implants to approximately 1.5 mm in length, and the implant heads were polished carefully. Implant dimensions and heads were examined and measured with a caliper under a stereomicroscope. Subsequently, implants were cleaned by sonicating for 45 minutes each in acetone, deionized water, and ethanol solutions, followed by sterilization in an autoclave.

Surgical Protocol for Implant Placement

Animals at the age of 11 weeks with a weight ranging between 27 and 30 g were subjected to implant placement surgery (Fig 1). Mice were anesthetized by inhalation of 4% isoflurane followed by an intramuscular (IM) injection of ketamine and xylazine (50–100 mg/kg; 20–50 mg/kg). Animals were placed on a surgical table, and surgeries were performed with the aid of a stereomicroscope.[18] Local administration of lidocaine (20 mg/mL with 1:100,000 epinephrine) was performed in the surrounding oral mucosa for additional pain control.

The maxillary right first molar of each mouse was extracted with minimal trauma by using a rat tooth forceps for molar luxation and removal. Immediately after tooth extraction, the residual medial root alveolar socket was used as the implant bed because it provides sufficient space for implant placement. A 0.45-mm pilot drill was used for the refined implant bed preparation. A microneedle holder (Fine Science tools) was used for implant installation.[18] The left first molar was used as the baseline control side for comparison of parameters measured in the implant side. After implant placement, animals were administered buprenorphine SR 1.25 mg/kg via subcutaneous administration for postsurgical analgesia. Mice were allowed to move freely after implantation and were provided free access to water and a softened diet for 72 hours after surgery. Feeding, drinking, grooming, and body weight were monitored daily

during the postoperative period. At 7 and 21 days after implant placement, ND and D mice were euthanized by an overdose of sodium pentobarbital. After euthanasia, the maxillae and pancreata were collected and fixed in 10% neutral-buffered formalin for further microscopic analysis.

MicroCT Imaging and Analysis

At least six maxillae from each time point (7 days and 21 days) and experimental group (ND and D) were scanned with ultra-high-resolution microCT imaging (OI-CT, MILabs). Samples were imaged at a voltage of 50 kV, a current of 0.21 mA, and an exposure time of 75 milliseconds. Projections were reconstructed with vendor software and converted to DICOM files using PMOD Technologies analysis software at a voxel size of 20 µm. Imalytics Preclinical (Gremse-IT) was used to visualize and quantify the region of interest surrounding the Ti implants. Analysis included acquisition of the bone volume fraction (BV/TV, %) in the alveolar socket of the first vestibular root, as well as surrounding the Ti implant, following the methodology previously described.[18]

Histologic processing and staining

After microCT scanning, bone samples were washed in tap water and subsequently immersed in 10% ethylenediaminetetraacetic acid disodium (EDTA Na^2) at room temperature. The EDTA solution was changed twice per week for 2 weeks for sample decalcification. Tissue processing was performed with the implant in place and prior to embedding samples in paraffin blocks. To avoid disturbing the morphology of implant-adherent cells, implants were unscrewed from their coronal portion carefully with a microneedle holder to obtain histologic semi-serial sections (5-µm thick) from the alveolar sockets and the implant area.[26] Ten sets of four serial sections were obtained from each biologic replicate. Samples were stained with hematoxylin and eosin (H&E) and Goldner Trichrome (GT) stain.[27] In addition to bone samples, the pancreata from both ND and D mice underwent tissue processing and paraffin embedding for histologic staining with H&E.

Histopathologic and Histomorphometric Analysis

The outcomes of socket healing and osseointegration were evaluated for histomorphometry and bone-to-implant contact (BIC, %) with H&E and GT stain, respectively. For histomorphometry, three technical replicates (sections) were evaluated with six histologic fields per section. Histologic fields captured at 400× magnification containing the interface of tissue surrounding the implant space were used to quantify the following parameters: blood vessels, inflammatory infiltrate, foreign body giant cells (FBGCs), fibroblasts and fibers, bone matrix, osteoblasts, and osteoclasts. In brief, a grid image containing a total of 100 points was superimposed on each histologic field with ImageJ software (version 1.51, National Institutes of Health). Histologic parameters within intersections were quantified and the total number of points was obtained to calculate the area density for each parameter (Table 1).

Table 1 Histomorphometric Analysis in H&E-Stained Samples

Parameter (area density, %)	Group	7 days (mean ± SD)	21 days (mean ± SD)
Bone Matrix	ND	35.80 ± 13.33[a]*	69.25 ± 7.80[b]*
	D	11.60 ± 10.74[a]*	21.60 ± 12.18[a]*
Osteoclasts	ND	1.80 ± 3.03[a]	0.02 ± 0.00[a]
	D	3.08 ± 2.95[a]	3.30 ± 4.99[a]
Inflammatory infiltrate	ND	5.00 ± 3.67*	0.70 ± 0.83*
	D	19.20 ± 6.38*	20.00 ± 12.88*
Fibers + Fibroblasts	ND	16.20 ± 8.67[a]	3.00 ± 3.83[a]
	D	27.60 ± 9.83[a]	15.40 ± 10.53[a]

[a, b] represent significant differences between time points within the same group; * represents significant difference between ND and D animals within the same time point when comparing between columns.

The best representative section of the 21-day time point was stained with GT and used to measure BIC% as previously described.[26,28] In brief, BIC was obtained using cellSens software (Olympus) to quantify the distance of the alveolar bone in direct contact with the implant (defined by implant space) and the entire length of the implant at the bone level. BIC% was determined by calculating the percentage of bone contact relative to the entire implant length at bone level. Data from histomorphometry and BIC were analyzed for statistical significance, and results were presented as mean ± standard deviation (SD).

Immunohistochemistry

Immunohistochemistry was used to identify and quantify markers related to angiogenesis and stem cells (CD146), proliferation (PCNA), macrophages (F4/80), and osteoblast differentiation (Runx2) in peri-implant tissues. Sections were deparaffinized and incubated with citrate buffer (pH 6.0) for antigen retrieval at 95°C for 30 minutes. Subsequently, tissue samples were blocked with protein block incubation. Primary antibody F4/80 (PA5-32399) was obtained from Invitrogen and diluted at 1:100. Other primary antibodies obtained from Abcam were diluted in the following concentrations: CD146 (ab228540) at 1:100; PCNA (ab92552) at 1:1,000; and Runx2 at 1:500 (ab236639). Samples were incubated overnight in a humidified chamber with each primary antibody at 4°C. Primary antibodies from

Table 2 Markers Identified by Immunohistochemical Analysis in D and ND Mice

Parameter (area density, %)	Group	7 days (mean ± SD)	21 days (mean ± SD)
Vessels (CD146+ cells)	ND	5.70 ± 1.86[a]	3.40 ± 2.51[a]
	D	3.40 ± 2.51[a]	5.67 ± 3.50[a]
Macrophages (F4/80+ cells)	ND	6.50 ± 3.27[a]	2.67 ± 2.16[a*]
	D	10.50 ± 3.93[a]	11.50 ± 3.91[a*]
Osteoblasts (Runx2+ cells)	ND	9.08 ± 4.76[a*]	3.75 ± 4.07[b]
	D	5.32 ± 4.04[a*]	1.67 ± 2.61[b]
Proliferation (PCNA+ cells)	ND	9.09 ± 4.26*	N/A
	D	5.52 ± 4.30*	N/A

[a, b] represent significant differences between time points within the same group; * represents significant difference between ND and D animals within the same time point when comparing between columns.

Abcam were subsequently incubated with rabbit-specific HRP/DAB (ABC) and the Micropolymer Detection IHC Kit (Abcam). At least four technical replicates from each sample were stained with each marker. A negative control was incubated with 1% bovine serum albumin in 1X PBS (Sigma-Aldrich) instead of a primary antibody. After incubation, the slides were washed and incubated with hydrogen peroxide solution for 10 minutes, washed three times in 1X PBS, and then incubated with the Micropolymer Abcam IHC kit. Lastly, slides were incubated for 1 minute with 3,3'-diaminobenzidine (DAB) chromogen and counterstained in Mayer's Hematoxylin for 2 minutes. Quantification of positive (+) cells for each marker was performed using the same technique employed with H&E-stained sections (Table 2).

Statistical Methods

Statistical analyses of FPGL, microCT data, BIC%, histomorphometry, and immunohistochemistry were tested for distribution with Shapiro-Wilk normality test. Nonparametric data was evaluated using Mann-Whitney *U* nonparametric test. Samples within normal distribution were analyzed using *t* test. Mann-Whitney or *t* test was used for comparisons to appraise the significance between time points within a group (eg, ND 7 days vs ND 21 days) and between treatments (eg, ND 21 days vs D 21 days). Statistical analysis was performed with GraphPad Prism 9.0 software (GraphPad Software). A *P* value of .05 or lower was considered statistically significant.

RESULTS

Diabetes Induction and Clinical Outcomes After Implant Surgery

Overall, 12 out of the 15 mice in the D group presented FPGLs of 265.30 ± 15.28 mg/dL at 7 days after IP injection of the last dose of STZ, while 3 mice presented values < 250 mg/dL and were excluded from the study. ND mice treated with 1X PBS (n = 3) presented FPGLs of 111.00 ± 4.36 at 7 days after IP injection, with no statistically significant differences compared to ND controls (88.67 ± 3.25, n = 6). Animals from ND and D groups were distributed into two experimental periods (7 and 21 days) after implant placement, with at least six animals/group for each time point. At 21 days after implant placement (30 days post-STZ injection), D group mice presented FPGLs of 344.70 ± 87.00 (n = 6) compared to 103.30 ± 14.98 for ND mice (n = 8). Histologic samples from ND and D pancreata were stained with H&E and analyzed for histopathologic changes in islets containing insulin-secreting beta cells. While normal and large pancreatic islets were observed in ND mice, significant atrophy and vacuolation were found in the pancreatic islets of all D mice.

From a clinical perspective, both ND and D mice exhibited clinical signs of mucosa healing at 7 days after implantation, with the screw head and remaining dental sockets covered by fibrin. Animals presented no weight loss or signs of hyperalgesia and exhibited normal grooming, eating, and nesting activities. At 21 days, oral epithelium covered the implants in both the ND and D groups (except for in two out of six animals from D group that presented partial implant exposure). Significant signs of inflammation, redness, and swelling were also found in implant sites in D mice.

MicroCT, BIC, and Histologic Analysis

Following microCT analysis of the remaining alveolar sockets and implant sites, increased hyperdensity was observed at 7 and 21 days, resulting in BV/TV (%) in the alveolar sockets of ND mice at 21 days of 68.88 ± 7.07 compared to 44.40 ± 6.98 in D mice. Quantitative evaluation of the bone surrounding the Ti implants also revealed an increase in BV/TV (%) at 21 days in ND mice compared to D mice (53.39 ± 5.93 and 46.08 ± 3.18, respectively) (Fig 2).

To better evaluate the limits of implant screws at the bone level and in relation to other anatomical structures (eg, the maxillary sinus or peri-implant mucosa), bone deposition and BIC were evaluated using histologic sections stained with GT. At 7 days after implantation, there was osteoid deposition surrounding the Ti spaces in the ND mice, whereas discrete bone formation was noted in the D mice. An increased quantity of inflammatory cells

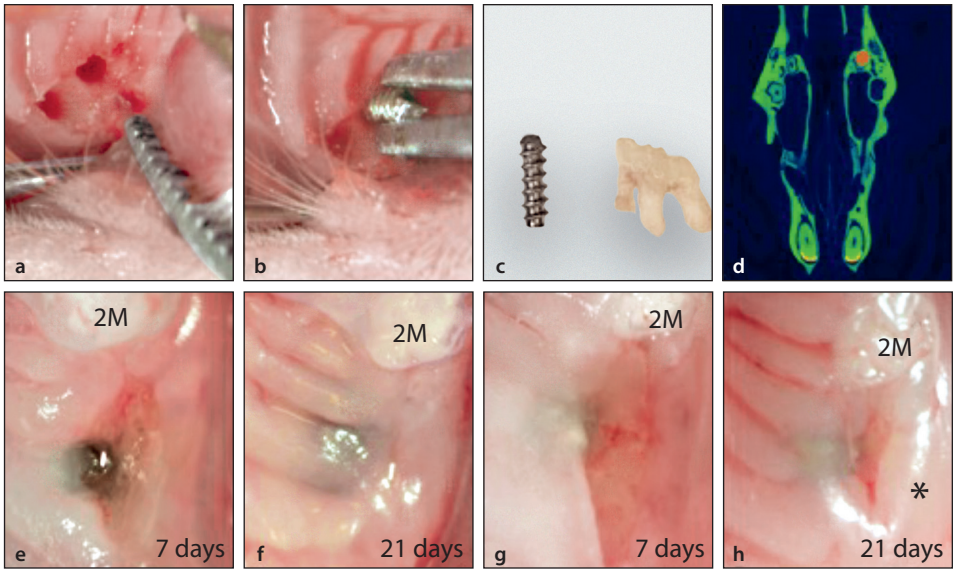

Fig 2 Overview of the surgical protocol and mucosal healing in 129/Sv mice. *(a)* Extraction of the mandibular first molar of the mouse, followed by *(b)* implant placement at the alveolar socket with microneedle holders. *(c)* Size of the implant in comparison to the molar roots. *(d)* MicroCT imaging of coronal sections of the alveolar sockets and implantation sites *(red)*. *(e)* ND group maxillary healing at 7 days and *(f)* 21 days. *(g)* D group maxillary healing at 7 days and *(h)* 21 days.

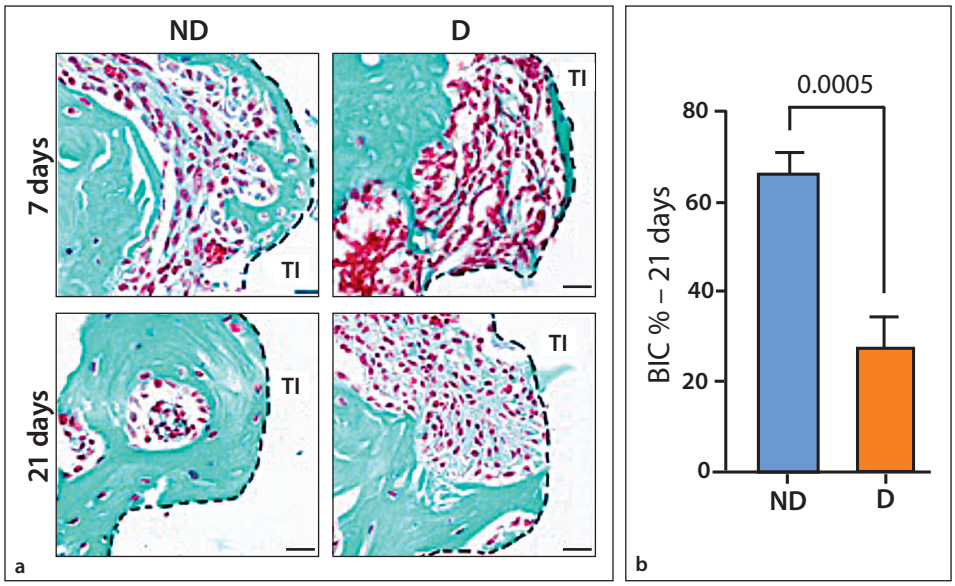

Fig 3 *(a)* Histologic evaluation of peri-implant sites in ND and D mice at 7 and 21 days after implant placement. *(b)* BIC% quantification at 21 days shown as mean ± SD at the implant site.

was also observed in the D animals. At 21 days, bone maturation was evident and predominant in ND mice, with 66.91% ± 12.50% BIC, while D mice maintained chronic inflammation with 28.13% ± 17.73% BIC (Fig 3). BIC was analyzed only at 21 days because there was no mature bone formation at 7 days.

Histologic evaluation with H&E-stained samples revealed that alveolar bone support was present in both ND and D mice. The implant screw was placed in the residual alveolar socket of the palatine root, within the apical limits of alveolar bone. After 7 days, implantation sites still exhibited areas of advanced bone formation in ND mice, with 35.80% ± 13.33% of area density occupied by bone matrix compared to 11.60% ± 10.74% in D mice ($P < .02$). There were still thread spaces with loosely packed connective tissue at the mucosa and bone level in the ND mice but reduced amounts of inflammatory infiltrate compared to D mice (5.00 ± 3.67 and 19.20 ± 6.38, respectively). Yet at 7 days, bone remodeling units were identified in alveolar sockets and implant sites, with multinucleated osteoclasts at the edge of the supporting bone, neighboring new cuboid osteoblasts aligned at the surface of the new and old bone matrices.

It was noted that the ND group presented a significant decrease in inflammatory infiltrate and a significant increase in newly formed bone matrix at 21 days after implantation compared to 7 days. On the other hand, four out of six implants from the D mice at 21 days were predominantly encapsulated by fibrous tissue with chronic inflammatory infiltrate in the thread spaces. Two D mice showed areas containing bone formation at the threads or in the residual alveolar socket.

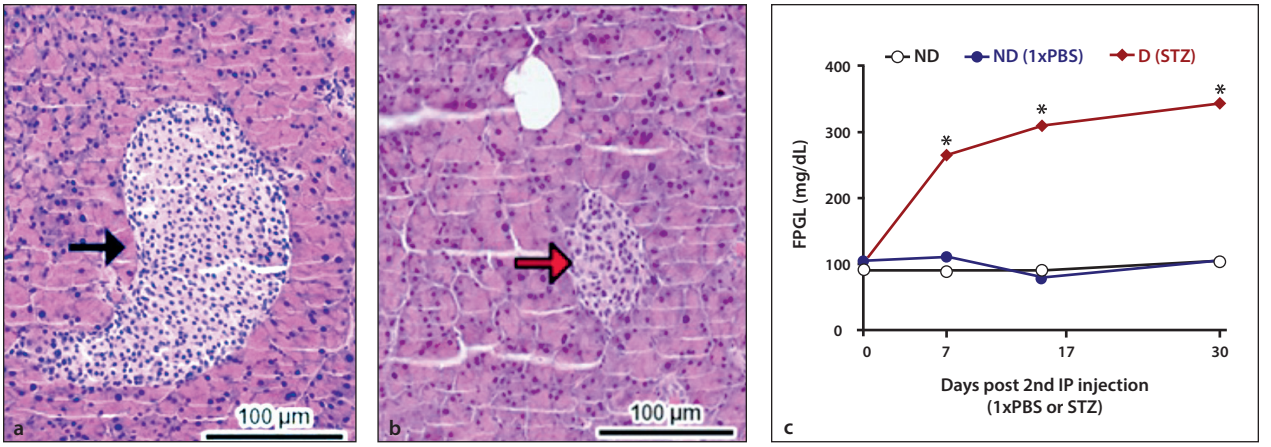

Fig 4 Histologic evaluation of pancreatic samples in ND *(a)* and D *(b)* mice 21 days after implant placement. The *black arrow* shows normal pancreatic islet–containing insulin-secreting beta cells and blood vessels in ND mice. The *red arrow* shows atrophic pancreatic islet in group D mice. *(c)* Mean FPGLs (mg/dL) measured over time in ND (n = 6), ND treated with 1X PBS (n = 3), and D mice (n = 12). * Indicates statistical significance as compared to both ND control groups ($P < .05$).

Immunohistochemical Analysis

Following immunohistochemical analysis, markers for angiogenesis (CD146+ cells), osteoblast differentiation (Runx2+ cells), macrophages (F4/80+), and proliferation (PCNA+ cells) were evaluated.

At the peri-implant mucosa level, both ND and D mice presented vessel formation, with loose connective tissue populated with fibroblast and mononuclear cells at 7 days. No significant differences were found in the quantity of blood vessels, although the characteristics of ND and D tissues permeated by blood vessels were different. In ND animals, CD146+ cells forming blood vessels were found close to new bone formation areas (at 7 days) and within bone marrow spaces (at 21 days). In group D, the abundance of CD146+ cells were found in the chronic inflammatory infiltrate and fibrous capsule (at 7 and 21 days).

Regarding F4/80+ macrophages, both ND and D mice presented a negligible quantity of positive cells. Some osteoclasts also stained positive for F4/80 marker but were not considered in the quantification. The quantity of F4/80+ macrophages was significantly increased in D group mice compared to ND mice at 21 days (11.50 ± 3.91 and 2.67 ± 2.16, respectively).

Runx2+ cells were abundant in the peri-implant areas of ND mice at 7 days (9.08 ± 4.76). In contrast, D mice presented significantly lower densities of Runx2+ cells (5.32 ± 4.04), with niches neighboring the edges of supporting alveolar bone. In ND mice, a significant decrease was observed from days 7 to 21, when Runx2 was found in resting osteoblasts surrounding mature bone. No differences were found between ND and D mice at 21 days. Similarly, ND mice also presented higher numbers of PCNA+ cells at 7 days (9.09 ± 4.26) compared to D mice (5.52 ± 4.30).

DISCUSSION

Considering the growing numbers of diabetic adults worldwide[1] and the current high demand for dental implant treatments,[29] implantologists are likely to treat diabetic patients more frequently than in the past. This study aimed to characterize the early oral osseointegration process in a 129/Sv diabetic mouse model to better explore the cellular dynamics involved in impaired early Ti osseointegration under chronic hyperglycemia.

According to the literature, DM in humans is characterized by inadequate beta cell response and insulin resistance, which leads to increased blood sugar levels or hyperglycemia.[1] There is a variety of diabetic rodent models, including the combination of an HFD with multiple doses of STZ, which mimics type 2 DM development.[23,30] An HFD may contribute to inducing insulin resistance overtime, which is one aspect of DM. Associated with multiple low-dose injections of STZ, this promotes a gradual impairment of pancreatic beta cells, culminating in a complete DM phenotype.[30] In this study, the continuous administration of an HFD from the age of 6 weeks was used, followed by two spaced IP injections of STZ when the animals reached 10 weeks of age. As a result, 3 out of 15 animals (20%) were pre-diabetic at day 7 after the last dose of STZ (with values ranging from 200 to

249 mg/dL). The remaining 12 animals were fully diabetic, presenting FPGLs > 249 mg/dL (Fig 4). It is important to consider that normal, pre-diabetic and diabetic FPGLs are significantly different between rodents and humans. In rodents, FPGLs < 199 mg/dL may be considered normal,[25] while in humans, the World Health Organization consider FPGLs of 126 mg/dL or above (given two separate measurements) as a diagnosis of DM.[31] To standardize the animals' ages for implant placement, the three prediabetic animals were not used for implant surgeries. In addition, three ND mice received an IP injection using only a cold vehicle to investigate the effects of IP injections on FPGLs. This procedure was not enough to provoke changes in FPGLs over time, and these animals were used as ND mice. Finally, in this study, 129/Sv strain mice were used. The 129/Sv mouse strain is optimized for the induction of DM using an HFD and two consecutive doses of STZ (100 mg/kg).[23] In addition, 129/Sv mice present greater skeletal BV/TV compared to other classic inbred strains (eg, C57, DBA, C3H, and AKR),[32] which may be an important factor of primary implant stability in this oral implant model.

Models of oral osseointegration in mice may vary according to the time points selected for analysis and the location of implant placement[33] according to the diastema between the maxillary incisors and first molar[18,34] or following the extraction of multiple teeth.[34] In the present study, it was demonstrated that the alveolar socket of the first molar palatal root may serve as a suitable implant bed for immediate implant placement (see Figs 1a, 2a, 2b). This procedure mimics the clinical approach of immediate implant placement into a fresh socket,[35] while allowing more bone surrounding the Ti screw for primary stability. Using the diastema avoids the trauma of tooth extraction, but the implant may protrude through the maxillary sinus.[18,33] In comparison to other models of implant placement after the extraction[34] of multiple teeth, this present model may be less traumatic and more accurate because the implant is installed in the same session and consistently in the same location (palatal root), avoiding secondary surgeries and longer procedures.[34,36] (Furthermore, it is crucial to shorten avoidable experimental periods and secondary surgeries when using diabetic animals because prolonging the life of the animal may cause unnecessary animal suffering and losses due long-term hyperglycemia complications.)[37] Therefore, single-stage surgery and maximum of 31 days after the last dose of STZ was the protocol of choice in this study, with all D animals remaining under chronic hyperglycemia but with none of the systemic complications that may occur 2 to 3 months after developing the disease.

Signs of clinical inflammation were evident in D mice at 21 days, but not in ND mice. Following microCT analysis at 21 days, a significant decrease in the proportion of mineralized bone at the alveolar sockets and peri-implant spaces of D mice was observed compared to ND (see Fig 1). This reduction also reflected a significant decrease in BIC in D mice compared to in ND mice (see Fig 3). Interestingly, no differences in supporting bone or stability were found between ND and D during the Ti screw placement. In the face of these clinical and subclinical observations, it is possible to infer that chronic hyperglycemia was associated with the inflammatory events leading to the impairment of osseointegration after Ti placement in the D mice. The microCT and BIC data here reflect other types of early osseointegration failure observed in previous studies, where either corrosion of the implant[28] or the inhibition of inflammatory mediators[20] induced the dysregulation of early healing events, which further affected subsequent processes leading to osseointegration.

Next, a detailed histologic analysis in H&E was performed, followed by immunohistochemistry analysis for different markers involved in healing (Figs 5 and 6). It has been well established in previous preclinical studies that the events occurring during the early stages after Ti placement influence the nature of the inflammatory response and support the first events of vascularization and osteogenesis.[38] In theory, host mediators present at the Ti-bone interface, as well as adsorbed to the Ti surfaces, will dictate the subsequent processes that lead to osseointegration, such as the role of growth factors and immunologic mediators[20,38] that orchestrate cell migration, proliferation, and differentiation in the peri-implant space.[39]

In the histologic analysis, it was possible to confirm signs of inflammation in ND mice at 7 days, but it was significantly lower than inflammation in the D mice. The area density of general inflammatory infiltrate (mononuclear and polymorphonuclear leukocytes) was significantly increased in D mice at 7 days and 21 days, while ND animals presented discrete inflammation at 7 days, which was completely resolved by day 21. The quantities of macrophages (F4/80+) in ND mice were also slightly higher at 7 days and decreased at 21 days. Macrophages play an important role in clearing cell debris and potential pathogens after tissue injury and also regulate both pro- and anti-inflammatory responses according to their state of polarization.[40] Upon hyperglycemia, monocytes/macrophages induce defective chemotaxis, phagocytosis, polarization, and suppression in cytokine production (eg, IL-2, IL-6 and IL-10).[2] In the present study, numbers of F4/80+ macrophages were significantly higher in D mice at 7 and 21 days, pointing to a dysregulated response of these cells in the peri-implant tissues.

In ideal conditions (ie, the absence of infection, necrotic bone, and hyperglycemia), the supporting bone

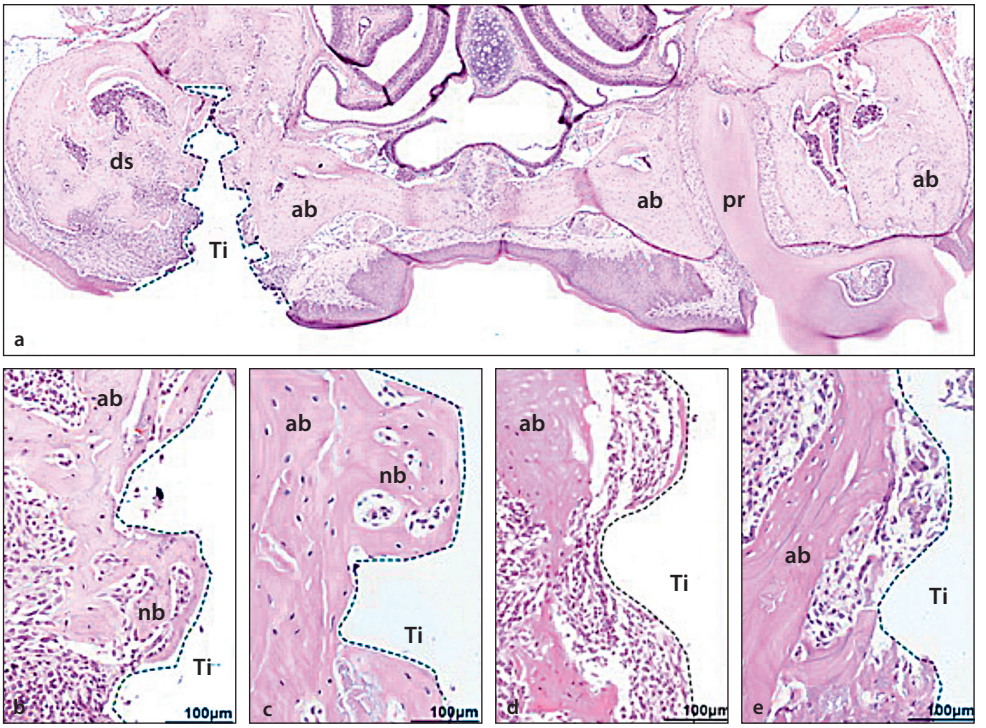

Fig 5 Histologic evaluation of H&E-stained peri-implant sites in ND and D mice at 7 and 21 days after implant placement. *(a)* Panoramic view of a transversal section of ND mice maxillae at 7 days after implant placement. Implant space (Ti) is demonstrated between the *dashed lines*. Peri-implant tissues at 7 *(b)* and 21 *(c)* days in ND mice and 7 *(d)* and 21 *(e)* days in D mice. ab: alveolar bone; nb: new bone; Ti: Ti implant space; pr: palatine root; ds: dental socket.

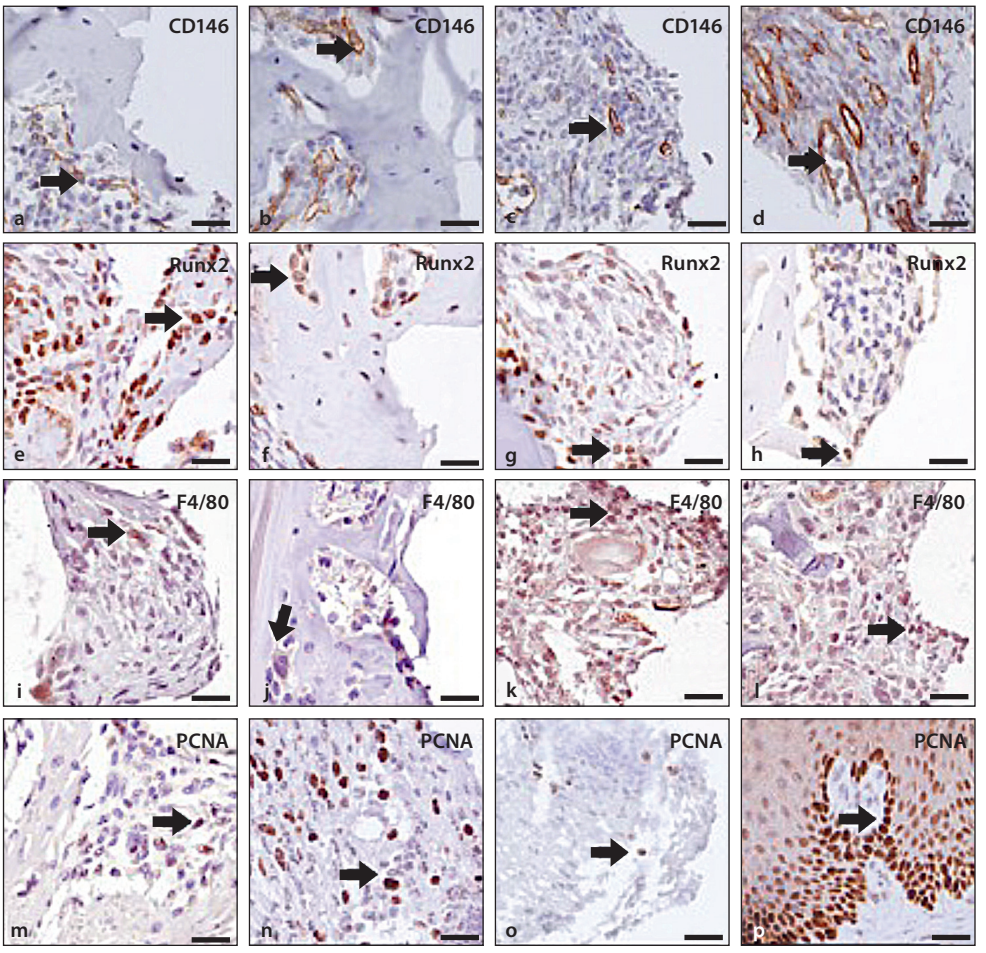

Fig 6 Immunohistochemistry for CD146 *(a to d)*, Runx2 *(e to h)*, F4/80 *(i to l)*, and PCNA *(m to p)* markers at the implant sites. Groups and time points are displayed as follows: ND 7 days *(a, e, i, and m)*, ND 21 days *(b, f, and j)*, D 7 days *(c, g, k, n, and o)*, D 21 days *(d, h, and l)*, positive control for PCNA in ND 7 days *(p)*. *Black arrows*: positive labeling. All samples incubated in chromogen DAB and counterstained with Mayer's hematoxylin (scale bar = 20 µm).

and the earlier granulation tissue at the Ti-host interface serves as a preosteoblastic supportive connective tissue.[33] Concomitantly with the resolution of inflammation at 7 days, ND mice presented bone differentiation activity that could be directly confirmed by the presence of new osteoid surrounding the Ti space at 7 days (see Figs 3 and 5) and the increased expression of Runx2+ cells. Also, the area density of Runx2 and PCNA-positive cells were significantly increased as compared to D mice at 7 days. The transcription factor Runx2[41] directly binds to enhancer regions of osteoblast-specific genes, and it regulates the commitment, proliferation, differentiation, and functions of osteoblasts, for example, upregulating the expression of several bone matrix protein genes.[42] In the present study, a significant decrease in the numbers of MSCs committed to osteoblastic differentiation (Runx2+ cells) in D mice was observed at 7 days compared to ND mice. The reduced density of PCNA+ cells in diabetic peri-implant sites further impairs osteoblast proliferation and function in these animals. Indeed, chronic hyperglycemia decreases the availability of cell progenitors and their recruitment into healing sites, reduces osteoblast differentiation, and decreases the quality of bone architecture and biomechanical properties.[16] Compared to nondiabetic persons, bone formation is decreased in diabetic persons, especially in patients with type 2 DM, as evidenced by the reduction in circulating osteogenic precursors (reduced molecular expression of the osteoblast regulator gene Runx2) and the reduced surface area of mineralized matrix and bone formation rates in diabetic women,[43] as well as lower serum levels of osteoblast markers in the serum of diabetic patients.[44,45]

In line with healing events, angiogenic activity is expected at earlier stages of osseointegration. Previous studies have shown that the adhesion molecule CD146 is expressed by vascular endothelial cells, MSCs, and pericytes.[46] Interestingly, no differences were found between CD146+ cell counts in the peri-implant spaces of the D and ND mice. In ND mice, CD146+ was found in vessels surrounding new bone formation at 7 days and in bone marrow spaces at 21 days. Of note, intense positive labeling was observed for CD146 cells in the peri-implant spaces of D mice, within vessels permeating areas of chronic inflammatory infiltrate, and in loose connective tissue at the Ti thread. Indeed, previous studies have demonstrated the CD146 expression is upregulated in endothelial cells in proinflammatory conditions, which may explain the presence of CD146+ cells in inflammatory regions of the peri-implant spaces of the D mice.[47,48]

In an observational clinical study comparing the profile of CD146+ pericytes isolated from the human bone marrow of diabetic and nondiabetic individuals, it was found that DM led to pericyte dysfunction but did not alter the number of CD146+ cells.[49] Interestingly, there is a diversity of CD146+ cells because CD146+ pericytes, which are prone to differentiate into osteoblasts, originate from the periosteum, whereas pericytes migrating from soft tissues do not undergo osteoblastogenesis.[50] One of the differences in CD146+ pericytes with skeletogenic potential is increased CXCR4 signaling, which is not found in pericytes from the soft tissues.[50] Based on these differences, it is reasonable to hypothesize that the increased numbers of CD146+ pericytes found in the D mice do not have osteogenic potential and may originate from the soft tissues. Therefore, it may be useful to identify the profile and origin of CD146+ cells in both D and ND peri-implant tissue in future studies.

Finally, it is important to emphasize that the method of titanium screw removal for histologic preparation may create some artifacts and remove some cells in proximity to the Ti surface. This is a limitation of this study and needs to be taken in consideration when evaluating stem cells and inflammatory cells. This is particularly important at the early time points.

CONCLUSIONS

In summary, this study evaluated immediate oral implant placement in 129/Sv diabetic mice and used specific healing markers to identify changes in the dynamics of cellular events involved in early oral osseointegration. By using microtomographic, histomorphometric, and immunohistochemical evaluation methods, this model may serve as tool for the evaluation of new materials and surface coatings to improve osseointegration in diabetic conditions.

ACKNOWLEDGMENTS

The authors thank Jimena Mora from the University of Texas for helping with histologic staining. C.B. thanks the Academy of Osseointegration/Osseointegration Foundation for its support. D.R. thanks the University of Texas at Dallas (UTD) Office of Research for the seed grant, the Collaborative Biomedical Research Award (CoBRA), and the National Institute of Dental & Craniofacial Research (NIDCR) 1R01DE026736-01A1. The authors declare they have no conflicts of interest related to this study.

REFERENCES

1. Cho NH, Shaw JE, Karuranga S, et al. IDF Diabetes atlas: Global estimates of diabetes prevalence for 2017 and projections for 2045. Diabetes Res Clin Pract 2018;138:271–281.
2. Berbudi A, Rahmadika N, Tjahjadi AI, Ruslami R. Type 2 diabetes and its impact on the immune system. Curr Diabetes Rev 2020;16:442–449.
3. Janghorbani M, Van Dam RM, Willett WC, Hu FB. Systematic review of type 1 and type 2 diabetes mellitus and risk of fracture. Am J Epidemiol 2007;166:495–505.

4. Morris HF, Ochi S, Winkler S. Implant survival in patients with type 2 diabetes: Placement to 36 months. Ann Periodontol 2000;5:157–165.
5. Olson JW, Shernoff AF, Tarlow J, Colwell J, Scheetz J, Bingham S. Dental endosseous implant assessments in a type 2 diabetic population: A prospective study. Int J Oral Maxillofac Implant 2000;15:811–818.
6. Wagner J, Spille JH, Wiltfang J, Naujokat H. Systematic review on diabetes mellitus and dental implants: An update. Int J Implant Dent 2022;8:1.
7. Javed F, Romanos GE. Impact of diabetes mellitus and glycemic control on the osseointegration of dental implants: A systematic literature review. J Periodontol 2009;80:1719–1730.
8. Wu JC, Huang WC, Tsai HW, et al. Pedicle screw loosening in dynamic stabilization: Incidence, risk, and outcome in 126 patients. Neurosurg Focus 2011;31:E9.
9. Kotsovilis S, Karoussis IK, Fourmousis I. A comprehensive and critical review of dental implant placement in diabetic animals and patients. Clin Oral Implants Res 2006;17:587–599.
10. Naujokat H, Kunzendorf B, Wiltfang J. Dental implants and diabetes mellitus—A systematic review. Int J Implant Dent 2016;2:5.
11. Maycas M, McAndrews KA, Sato AY, et al. PTHrP-derived peptides restore bone mass and strength in diabetic mice: Additive effect of mechanical loading. J Bone Miner Res 2017;32:486–497.
12. Murray CE, Coleman CM. Impact of diabetes mellitus on bone health. Int J Mol Sci 2019;20:4873.
13. Napoli N, Chandran M, Pierroz DD, Abrahamsen B, Schwartz AV, Ferrari SL. Mechanisms of diabetes mellitus-induced bone fragility. Nat Rev Endocrinol 2017:208–219.
14. Schneider ALC, Williams EK, Brancati FL, Blecker S, Coresh J, Selvin E. Diabetes and risk of fracture-related hospitalization: The atherosclerosis risk in communities study. Diabetes Care 2013;36:1153–1158.
15. Kolluru GK, Bir SC, Kevil CG. Endothelial dysfunction and diabetes: Effects on angiogenesis, vascular remodeling, and wound healing. Int J Vasc Med 2012;2012:918267.
16. Doherty L, Wan M, Kalajzic I, Sanjay A. Diabetes impairs periosteal progenitor regenerative potential. Bone 2020;143:115764.
17. Vandamme TF. Use of rodents as models of human diseases. J Pharm Bioallied Sci 2014;6:2–9.
18. Biguetti CC, Cavalla F, Silveira EM, et al. Oral implant osseointegration model in C57Bl/6 mice: Microtomographic, histological, histomorphometric and molecular characterization. J Appl Oral Sci 2018;26:1–16.
19. Albertini M, Fernandez-Yague M, Lázaro P, et al. Advances in surfaces and osseointegration in implantology. Biomimetic surfaces. Med Oral Patol Oral Cir Bucal 2015;20:e316–325.
20. Biguetti CC, Cavalla F, Silveira EV, et al. HGMB1 and RAGE as essential components of Ti osseointegration process in mice. Front Immunol 2019;10:709.
21. Monje A, Catena A, Borgnakke WS. Association between diabetes mellitus/hyperglycaemia and peri-implant diseases: Systematic review and meta-analysis. J Clin Periodontol 2017;44:636–648.
22. Hasegawa H, Ozawa S, Hashimoto K, Takeichi T, Ogawa T. Type 2 diabetes impairs implant osseointegration capacity in rats. Int J Oral Maxillofac Implants 2008;23:237–246.
23. Nørgaard SA, Søndergaard H, Sørensen DB, Galsgaard ED, Hess C, Sand FW. Optimising streptozotocin dosing to minimise renal toxicity and impairment of stomach emptying in male 129/Sv mice. Lab Anim 2020;54:341–352.
24. Nørgaard SA, Sand FW, Sørensen DB, Abelson KS, Søndergaard H. Softened food reduces weight loss in the streptozotocin-induced male mouse model of diabetic nephropathy. Lab Anim 2018;52:373–383.
25. Fajardo RJ, Karim L, Calley VI, Bouxsein ML. A review of rodent models of type 2 diabetic skeletal fragility. J Bone Miner Res 2014;29:1025–1040.
26. Wheelis SE, Natarajan SA, Lakkasetter Chandrashekar B, Arteaga A, Garlet GP, Rodrigues DC. Effects of dicationic imidazolium-based ionic liquids on oral osseointegration of titanium implants: An in vivo biocompatibility study in multiple rat demographics. Genes (Basel) 2022;13:1–25.
27. Biguetti CC, De Oliva AH, Healy K, et al. Medication-related osteonecrosis of the jaws after tooth extraction in senescent female mice treated with zoledronic acid: Microtomographic, histological and immunohistochemical characterization. PLoS One 2019;14:e0214173.
28. Biguetti CC, Cavalla F, Fonseca AC, et al. Effects of titanium corrosion products on in vivo biological response: A basis for the understanding of osseointegration failures mechanisms. Front Mater 2021;8:159.
29. Elani HW, Starr JR, Da Silva JD, Gallucci GO. Trends in dental implant use in the U.S., 1999–2016, and projections to 2026. J Dent Res 2018;97:1424–1430.
30. Qian C, Zhu C, Yu W, Jiang X, Zhang F. High-fat diet/low-dose streptozotocin-induced type 2 diabetes in rats impacts osteogenesis and WNT signaling in bone marrow stromal cells. PLoS One 2015;10:e0136390.
31. Riley L. Mean fasting blood glucose. World Health Organization, 2022. https://www.who.int/data/gho/indicator-metadata-registry/imr-details/2380.
32. Sabsovich I, Clark JD, Liao G, et al. Bone microstructure and its associated genetic variability in 12 inbred mouse strains: MicroCT study and in silico genome scan. Bone 2008;42:439–451.
33. Mouraret S, Hunter DJ, Bardet C, Brunski JB, Bouchard P, Helms JA. A pre-clinical murine model of oral implant osseointegration. Bone 2014;58:177–184.
34. Pirih FQ, Hiyari S, Barroso AD V, et al. Ligature-induced peri-implantitis in mice. J Periodontal Res 2015;50:519–524.
35. Ebenezer V, Balakrishnan K, Asir RVD, Sragunar B. Immediate placement of endosseous implants into the extraction sockets. J Pharm Bioallied Sci 2015;7 (suppl 1):S234–S237.
36. Pirih FQ, Hiyari S, Leung HY, et al. A murine model of lipopolysaccharide-induced peri-implant mucositis and peri-implantitis. J Oral Implantol 2015;41:e158–e164.
37. Singh R, Farooq SA, Mannan A, et al. Animal models of diabetic microvascular complications: Relevance to clinical features. Biomed Pharmacother 2022;145:112305.
38. Thalji GN, Nares S, Cooper LF. Early molecular assessment of osseointegration in humans. Clin Oral Implants Res 2014;25:1273–1285.
39. Lin Z, Rios HF, Volk SL, Sugai JV, Jin Q, Giannobile WV. Gene expression dynamics during bone healing and osseointegration. J Periodontol 2011;82:1007–1017.
40. Mantovani A, Sica A, Sozzani S, Allavena P, Vecchi A, Locati M. The chemokine system in diverse forms of macrophage activation and polarization. Trends Immunol 2004;25:677–686.
41. Jonason JH, Xiao G, Zhang M, Xing L, Chen D. Post-translational regulation of Runx2 in bone and cartilage. J Dent Res 2009;88:693–703.
42. Komori T. Regulation of proliferation, differentiation and functions of osteoblasts by Runx2. Int J Mol Sci 2019;20:1694.
43. Manavalan JS, Cremers S, Dempster DW, et al. Circulating osteogenic precursor cells in type 2 diabetes mellitus. J Clin Endocrinol Metab 2012;97:3240–3250.
44. Shu A, Yin MT, Stein E, et al. Bone structure and turnover in type 2 diabetes mellitus. Osteoporos Int 2012;23:635–641.
45. Iglesias P, Arrieta F, Piñera M, et al. Serum concentrations of osteocalcin, procollagen type 1 N-terminal propeptide and beta-crosslaps in obese subjects with varying degrees of glucose tolerance. Clin Endocrinol (Oxf) 2011;75:184–188.
46. Bussard KM, Spaeth E, Mutkus LA, Stumpf KA, Marini FC. Mesenchymal stem cell transition to tumor-associated stromal cells contributes to cancer progression. Mesenchymal Stromal Cells as Tumor Stromal Modul 2017:253–273.
47. Abu El-Asrar AM, Nawaz MI, Ahmad A, et al. CD146/soluble CD146 pathway is a novel biomarker of angiogenesis and inflammation in proliferative diabetic retinopathy. Invest Ophthalmol Vis Sci 2021;62:32.
48. Fan Y, Fei Y, Zheng L, et al. Expression of endothelial cell injury marker CD146 correlates with disease severity and predicts the renal outcomes in patients with diabetic nephropathy. Cell Physiol Biochem 2018;48:63–74.
49. Mangialardi G, Ferland-McCollough D, Maselli D, et al. Bone marrow pericyte dysfunction in individuals with type 2 diabetes. Diabetologia 2019;62:1275–1290.
50. Xu J, Li D, Hsu C-Y, et al. Comparison of skeletal and soft tissue pericytes identifies CXCR4+ bone forming mural cells in human tissues. Bone Res 2020;8:22.